Industrial Mathematics Institute

2007:03

Numerical simulations of the steady Navier-Stokes equations using adaptive meshing schemes

L. Ju, H.-C. Lee and L. Tian

IMI

Preprint Series

Department of Mathematics
University of South Carolina

Numerical Simulations of the Steady Navier-Stokes Equations Using Adaptive Meshing Schemes

Lili Ju* Hyung-Chun Lee† Li Tian‡

Abstract

In this paper, we consider an adaptive meshing scheme for solution of the steady incompressible Navier-Stokes equations by finite element discretizations. The mesh refinement and optimiztaion are performed based on an algorithm that combines the so-call conforming centroidal Voronoi Delaunay triangulations and residual-type local a posteriori error estimators. Numerical experiments for various examples are presented with quadratic finite elements used for the velocity field and linear finite elements for the pressure. The results show that our meshing scheme can equally distribute the errors over all elements in a quite optimal way and keep the triangles very well shaped as well at all levels of refinement. In addition, the convergence rates achieved are close to the best obtainable.

keywords: Navier-Stokes equations, centroidal Voronoi tessellation, conforming centroidal Voronoi Delaunay triangulations, a posteriori error estimators

1 Introduction

In many scientific and engineering problems, one always desires increasing the accuracy of the approximate solutions without adding unnecessary degrees of freedom. Therefore, adaptive algorithm have been playing more and more important roles in the solution process, that allows one to refine the mesh in the critical regions while remaining reasonablely coarse in the rest of the domain. Two important ingredients of adaptive algorithm for the numerical solution of partial differential equations (PDEs) are the local error estimator and the mesh adaptivity scheme, see [7, 5, 6, 2, 3, 17, 15, 16, 20] and references therein. Here we are especially interested in the second ingredient. As point out in [14], for most current adaptive methods for PDEs, the meshes are only refined locally whenever some criterion based on a local error estimator is not satisfied on some elements; the mesh elsewhere in the domain is not changed. However, in an unrefined region, the errors could be so small that, because one has too many grid nodes there, computational resources are wasted.

Numerical solution of the Navier-Stokes equation has been one of central interests in the study of fluid mechanics in the past decades partially due to its many applications in various fields such as geophysics, atmospheric science, aerospace engineering and so on [19, 12]. In this paper, we propose an adaptive meshing scheme for numerical simulation of the steady incompressible Navier-Stokes

*Department of Mathematics, University of South Carolina, Columbia, SC 29208, USA. *Email:* ju@math.sc.edu. This work is partially supported by the National Science Foundation under grant number DMS-0609575 and the University of South Carolina Research and Productive Scholarship under grant number RPS-13060-06-12306.

†Department of Mathematics, Ajou University, Suwon, Korea 443-749. *Email:* hclee@ajou.ac.kr. This work was partially supported by grant No. R01-2006-000-10472-0 from KOSEF.

‡Department of Mathematics, University of South Carolina, Columbia, SC 29208, USA. *Email:* tianl@math.sc.edu.

equations (INSE), that can distribute the nodes in some optimal way according to local a posteriori error estimates, so that the error of the resulting approximate solution is distributed equally over the elements. The key of our algorithm is the use of a meshing scheme called *conforming centroidal Voronoi Delaunay trianglation* (CfCVDT) [13]. A similar methodology for the solution of second order elliptic PDEs was also proposed in [14]. The plan of the rest of the paper is as follows. We first give a short introduction to the steady INSE in the remaining of this section. In Sections 2, we then discuss its finite element discretization and a specific local a posteriori error estimator. In Sections 3, we propose our adapive meshing scheme that connects the the error estimators effectively with the CfCVDT mesh generator. In Section 4, several computational experiments in the two dimensional space are carried out to demonstrate the high efficiency of our mesh adaptation approach. Finally, some conclusions are given in Section 5. We also would like to remark that we are currently studying the extension of this methodology to problems in three dimensions.

1.1 Steady incompressible Navier-Stokes equations

Let us consider the model steady Navier-Stokes equations for incompressible flows in a bounded and connected region Ω in $\mathbb{R}^d$:

$$-\nu\triangle\mathbf{u}+(\mathbf{u}\cdot\nabla)\mathbf{u}+\nabla p = \mathbf{f} \quad \text{in } \Omega \tag{1.1}$$

$$\nabla\cdot\mathbf{u} = 0 \quad \text{in } \Omega \tag{1.2}$$

with boundary conditions

$$\mathbf{u}=\mathbf{g} \quad \text{on} \quad \Gamma_D, \quad \text{and} \quad (\mathbf{n}\cdot\nabla)\mathbf{u}=\mathbf{h} \quad \text{on} \quad \Gamma_N \tag{1.3}$$

where $\mathbf{u}\in\mathbb{R}^d$ represents the velocity and $p\in\mathbb{R}$ the pressure, and ν is the kinetic viscosity constant. The computational domain $\partial\Omega=\Gamma_D\cup\Gamma_N$ where the Dirichlet boundary Γ_D must have positive measure and the Neumann part Γ_N can be empty. The functions $\mathbf{g}\in\mathbf{H}^{1/2}(\Gamma_D)$ and $\mathbf{h}\in\mathbf{H}^{-1/2}(\Gamma_N)$ are given. For the pure Dirichlet boundary value problem ($\Gamma_N=\emptyset$), the boundary condition satisfies the following constraint:

$$\oint_{\partial\Omega}\mathbf{u}\cdot\mathbf{n}\,ds=0 \tag{1.4}$$

where $\mathbf{n}$ is the outer normal of $\partial\Omega$. Let us use the standard notation of Sobolev spaces and set

$$\mathbf{H}^1_D(\Omega)=(H^1_D(\Omega))^d \quad \text{and} \quad \mathbf{V}=\mathbf{H}^1_D(\Omega)\times L^2_0(\Omega)$$

where $\mathbf{H}^1_D(\Omega)=\{\mathbf{u}\in\mathbf{H}^1(\Omega)\mid\mathbf{u}=\mathbf{0}\text{ on }\Gamma_D\}$ and $L^2_0(\Omega)=\{q\in L^2(\Omega)\mid\int_\Omega q\,d\mathbf{x}=0\}$. We will use the same notation for the corresponding norm on $\mathbf{H}^1(\Omega)$ and $L^2(\Omega)$. Then define the following linear, bilinear, and trilinear functionals:

$$\begin{aligned}
&a:\mathbf{H}^1_D(\Omega)\times\mathbf{H}^1_D(\Omega)\to\mathbb{R}, && a(\mathbf{u},\mathbf{v})=\int_\Omega\nu\nabla\mathbf{u}\cdot\nabla\mathbf{v}\,d\mathbf{x}\\
&b:\mathbf{H}^1_D(\Omega)\times\mathbf{H}^1_D(\Omega)\times\mathbf{H}^1_D(\Omega)\to\mathbb{R}, && b(\mathbf{u},\mathbf{v},\mathbf{w})=\int_\Omega(\mathbf{u}\cdot\nabla)\mathbf{v}\cdot\mathbf{w}\,d\mathbf{x}\\
&c:L^2_0(\Omega)\times\mathbf{H}^1_D(\Omega)\to\mathbb{R}, && c(p,\mathbf{v})=\int_\Omega p\nabla\cdot\mathbf{v}\,d\mathbf{x}\\
&f:\mathbf{H}^{-1}(\Omega)\to\mathbb{R}, && f(\mathbf{v})=\int_\Omega\mathbf{f}\cdot\mathbf{v}\,d\mathbf{x}
\end{aligned}$$

The forms $a(\cdot,\cdot)$, $c(\cdot,\cdot)$ and $f(\cdot)$ are continuous and $c(\cdot,\cdot)$ satisfies the standard inf-sup condition [2, 17]. The trilinear form $b(\cdot,\cdot,\cdot)$ is also continuous and satisfies

$$\|b\|=\sup_{\mathbf{u},\mathbf{v},\mathbf{w}\in\mathbf{H}^1(\Omega)}\frac{b(\mathbf{u},\mathbf{v},\mathbf{w})}{|\mathbf{u}|_{1,\Omega}|\mathbf{v}|_{1,\Omega}|\mathbf{w}|_{1,\Omega}}<\infty.$$

Then the standard weak form of equations (1.1) and (1.2) is given by: find $(\mathbf{u}, p) \in \mathbf{V}$ such that

$$\mathcal{L}((\mathbf{u}, p), (\mathbf{v}, q)) = f(\mathbf{v}), \qquad \forall\, (\mathbf{v}, q) \in \mathbf{V}, \tag{1.5}$$

where

$$\mathcal{L}((\mathbf{u}, p), (\mathbf{v}, q)) = a(\mathbf{u}, \mathbf{v}) + b(\mathbf{u}, \mathbf{u}, \mathbf{v}) - c(p, \mathbf{v}) - c(q, \mathbf{u}). \tag{1.6}$$

Due to Temam's work [19], a stabilization term is often added into $b(\cdot, \cdot, \cdot)$ such that

$$b(\mathbf{u}, \mathbf{v}, \mathbf{w}) = \int_\Omega (\mathbf{u} \cdot \nabla)\mathbf{v} \cdot \mathbf{w} + \frac{1}{2}(\nabla \cdot \mathbf{u})\mathbf{v} \cdot \mathbf{w}\, d\mathbf{x}.$$

Note that the above $b(\mathbf{u}, \mathbf{v}, \mathbf{v}) = 0$ for all $\mathbf{u}, \mathbf{v} \in \mathbf{H}^1_D(\Omega)$ and this modification will not affect the solution of the problem (1.5).

In the following, we will also assume that the body force $\mathbf{f}$ belongs to $\mathbf{H}^{-1}(\Omega)$ and its norm is given by

$$\|\mathbf{f}\|_{-1,\Omega} = \sup_{\mathbf{v} \in \mathbf{H}^1(\Omega), \mathbf{v} \neq \mathbf{0}} \frac{f(\mathbf{v})}{|\mathbf{v}|_{1,\Omega}}.$$

Then we have the following results about the existence and uniqueness of problem (1.5):

Theorem 1 *Let Ω be a bounded Lipschitz domain in $\mathbb{R}^d$ ($d \leq 3$) and $\mathbf{f} \in \mathbf{H}^{-1}(\Omega)$. Then there exists at least one solution $(\mathbf{u}, p) \in \mathbf{V}$ to the problem (1.5). Moreover, if*

$$\|\mathbf{f}\|_{-1,\Omega} \leq \frac{\nu^2}{\|b\|}, \tag{1.7}$$

then the solution $(\mathbf{u}, p) \in \mathbf{V}$ is unique and satisfies the bound

$$\|\mathbf{u}\|_{1,\Omega} \leq \frac{1}{\nu}\|\mathbf{f}\|_{-1,\Omega} \leq \frac{\nu}{\|b\|}. \tag{1.8}$$

2 Finite Element Approximation of the INSEs

In the follwing section, we will introduce in brief finite element approximations of equation (1.5) and corresponding error estimates that will be used for our adaptive solution process.

2.1 Discretization and prior error estimates

Let $\Omega \in \mathbb{R}^d$ ($d \leq 3$) be a bounded Lipschitz domain and $\mathcal{T} = \{T_j\}$ be a conforming triangulation of Ω (T_j are triangles for $d = 2$ or tetrahedra for $d = 3$). Denote by h_T the diameter of the element $T \in \mathcal{T}$ and by r_T the diameter of the largest sphere that can be inscribed in T. We also assume that $\mathcal{T}$ is regular, i.e., there is a constant $\kappa > 0$ such that the ratio

$$\kappa_T = \frac{h_T}{r_T} \leq \kappa$$

for all $T \in \mathcal{T}$. Denote by $\mathbb{P}_k$ the space of polynomials of degree $\leq k$. Let us choose the following finite element spaces:

$$\begin{array}{rcl} \mathbf{Y}^h &=& \{\mathbf{v}^h \in (C(\overline{\Omega}))^d \;|\; \mathbf{v}^h|_{T_j} \in (\mathbb{P}_{k+1}(T_j))^d, \;\; \forall\, T_j \in \mathcal{T}\}, \\ \mathbf{X}^h &=& \{\mathbf{v}^h \in \mathbf{Y}^h \;|\; \quad \mathbf{v}^h|_{\partial\Omega} = \mathbf{0}\}, \\ M^h &=& \{q^h \in C(\overline{\Omega}) \;|\; q^h|_{T_j} \in \mathbb{P}_k(T_j), \;\; \forall\, T_j \in \mathcal{T}\}, \\ Q^h &=& \{q^h \in M^h \;|\; \int_\Omega q^h\, d\mathbf{x} = 0\}, \end{array} \tag{2.1}$$

and let $\mathbf{V}^h = \mathbf{X}^h \times Q^h$ be the pair of discrete spaces for the velocity filed and the pressure respectively. There exist mappings $\Pi_h \in \mathcal{L}(\mathbf{H}^2(\Omega), \mathbf{Y}^h) \cap \mathcal{L}(\mathbf{H}^2(\Omega) \cap \mathbf{H}^2_D(\Omega), \mathbf{X}^h)$ and $\pi_h \in \mathcal{L}(L^2(\Omega), M^h)$ such that

$$|\mathbf{v} - \Pi_h \mathbf{v}|_{1,\Omega} \leq ch^{l-m} \|\mathbf{v}\|_{l+1-m,\Omega}, \quad \forall\, \mathbf{v} \in \mathbf{H}^{l+1}(\Omega),$$
$$|q - \pi_h q|_{0,\Omega} \leq ch^{l-m} \|q\|_{l-m,\Omega}, \quad \forall\, q \in H^l(\Omega).$$

for $0 \leq m \leq l-1$ and $l \leq k+1$.

Then, a finite element discretization for the problem (1.5) can be obtained by: find $(\mathbf{u}^h, p^h) \in \mathbf{V}^h$ such that

$$\mathcal{L}((\mathbf{u}^h, p^h), (\mathbf{v}^h, q^h)) = f(\mathbf{v}^h), \qquad \forall\, (\mathbf{v}^h, q^h) \in V^h. \tag{2.2}$$

Especially, it is also called the Hood-Taylor discretization when $k = 1$. See Figure 1 for a description of P2-P1 Hood-Taylor element in two dimensions.

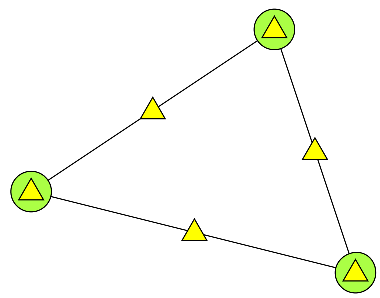

Figure 1: P2-P1 Hood-Taylor finite element where the triangles are the velocity nodes and the circles are the pressure nodes.

For any $(\mathbf{u}, p) \in \mathbf{V}$, let us define

$$|(\mathbf{u}, p)|_V = \left(|\mathbf{u}|^2_{1,\Omega} + \nu^{-2}|p|^2_{0,\Omega}\right)^{\frac{1}{2}} \tag{2.3}$$

Under reasonable conditions, the following prior error estimates can be established for the solution of discretization (2.2), see [12, 17].

Theorem 2 *Let Ω be a bounded Lipschitz domain in $\mathbb{R}^d$ $(d \leq 3)$ and $\mathbf{f} \in \mathbf{H}^{-1}(\Omega)$. Let $(\mathbf{u}, p)$ be the solution of problem (1.5). Then for ν sufficiently large, there exists an h^* such that for all $h \leq h^*$, problem (2.2) has a unique solution $(\mathbf{u}^h, p^h) \in \mathbf{V}^h$ and*

$$\lim_{h \to 0} |(\mathbf{u} - \mathbf{u}^h, p - p^h)|_V = 0.$$

In addition, if $(\mathbf{u}, p) \in (\mathbf{H}^{k+2}(\Omega) \cap \mathbf{H}^1_D(\Omega)) \times (H^{k+1}(\Omega) \cap Q(\Omega))$, then there exists a constant c independent of h, such that

$$|(\mathbf{u} - \mathbf{u}^h, p - p^h)|_V \leq ch^{k+1}. \tag{2.4}$$

2.2 A posteriori error estimates

The prior estimates often don't play an important role in adaptive algorithms since configurations of exact solutions are generally not clear. In this paper we will make use of a residual-based a posteriori error estimator for mesh refinement and optimization in our method.

Let $\mathcal{E}_I$ denote the set of interior edges (or faces) of $\mathcal{T}$. If two elements T and T' of $\mathcal{T}$ share the common edge (face) $\gamma \in \mathcal{E}_I$, define the jump in the normal flux of $\mathbf{u}^h$ across the edge γ by

$$\left[(\nu\nabla\mathbf{u}^h)\cdot\mathbf{n}_\gamma\right]_\gamma = (\nu\nabla\mathbf{u}^h)|_T\cdot\mathbf{n}_T + (\nu\nabla\mathbf{u}^h)|_{T'}\cdot\mathbf{n}_{T'}$$

where $\mathbf{n}_T$ is the unit outward normal vector to ∂T. Now set

$$\mathbf{r}_\gamma = \begin{cases} \left[(\nu\nabla\mathbf{u}^h)\cdot\mathbf{n}_\gamma\right]_\gamma & \text{if } \gamma\in\mathcal{E}_I, \\ 0 & \text{if } \gamma\in\partial\Omega, \end{cases} \tag{2.5}$$

and

$$\mathbf{R} = \mathbf{f} + \nu\triangle\mathbf{u}^h - (\mathbf{u}^h\nabla)\mathbf{u}^h - \frac{1}{2}(\nabla\cdot\mathbf{u}^h)\mathbf{u}^h - \nabla p^h. \tag{2.6}$$

Then for any $T\in\mathcal{T}$, a local a posteriori error estimator on T proposed in [2] is defined by

$$\eta_T = \left[|T|\|\mathbf{R}\|_{0,T}^2 + \nu^2\|\nabla\cdot\mathbf{u}^h\|_{0,T}^2 + \frac{1}{2}\sum_{\gamma\in\partial T}|\gamma|\|\mathbf{r}\|_{0,\gamma}^2\right]^{\frac{1}{2}} \tag{2.7}$$

where $|T|$ denotes the area (or volume) of T and $|\gamma|$ the length (or area) of γ.

An local error estimator is called *reliable* if the true error can be bounded from above in terms of the local error estimator, and *efficient* if the true error is also locally bounded from below by the local error estimator. The following result for η_T has been proved in [2].

Theorem 3 *For ν sufficiently large, the local error estimator η_T defined in (2.7) is reliable for the Hood-Taylor discretization ($d = 2$ and $k = 1$ for $\mathbf{X}^h$ and Q^h defined in (2.1)), i.e., there exists some contant c independent of h, such that*

$$|(\mathbf{u}-\mathbf{u}^h, p-p^h)|_V \le c\eta \tag{2.8}$$

where $\eta = \left(\sum_{T\in\mathcal{T}}\eta_T^2\right)^{1/2}$.

There is still no proof for the efficiency of the η_T yet, but it has been shown to be numerically very effective, see [2]. This local a posteriori estimator will be one of two essential ingredients used for mesh refinement and optimization in our adaptive algorithm. Of course, there are also other good a posteriori error estimators that can be used here, such as the ones proposed in [17, 20] and so on.

3 Adaptive Meshing Scheme

Another essential ingrdient of our adaptive method is a special meshing methodology, called *Centroidal Voronoi Tessellation* proposed in [8], that can effectively control the local mesh sizes by pre-defining some density (nodes distribution) function.

3.1 Conforming centroidal Voronoi Delaunay triangulations

Given an open bounded domain $\Omega\in\mathbb{R}^d$ and a set of distinct points $\{\mathbf{x}_i\}_{i=1}^n\subset\Omega$. For each point $\mathbf{x}_i$, $i=1,\ldots,n$, define the corresponding Voronoi region V_i, $i=1,\ldots,n$, by

$$V_i = \left\{\mathbf{x}\in\Omega \mid \|\mathbf{x}-\mathbf{x}_i\| < \|\mathbf{x}-\mathbf{x}_j\| \text{ for } j=1,\cdots,n \text{ and } \; j\neq i\right\}$$

where $\|\cdot\|$ denotes the Euclidean distance in $\mathbb{R}^d$. Clearly $V_i \cap V_j = \emptyset$ for $i \neq j$, and $\cup_{i=1}^n \overline{V}_i = \Omega$ so that $\{V_i\}_{i=1}^n$ is a tessellation of Ω. We refer to $\{V_i\}_{i=1}^n$ as the *Voronoi tessellation* (VT) of Ω associated with the point set $\{\mathbf{x}_i\}_{i=1}^n$. A point $\mathbf{x}_i$ is called a *generator*; a subdomain $V_i \subset \Omega$ is referred to as the *Voronoi region* corresponding to the generator $\mathbf{x}_i$. It is well-known that the dual tessellation (in a graph-theoretical sense) to a Voronoi tessellation of Ω is the so-called *Delaunay triangulation* (DT).

Given a density function $\rho(\mathbf{x}) \geq 0$ defined on Ω, for any region $V \subset \Omega$, define $\mathbf{x}^*$, the *centroid* of V by

$$\mathbf{x}^* = \frac{\displaystyle\int_V \mathbf{y}\rho(\mathbf{y})\, d\mathbf{y}}{\displaystyle\int_V \rho(\mathbf{y})\, d\mathbf{y}}. \tag{3.1}$$

Then we refer to a Voronoi tessellation $\{(\mathbf{x}_i, V_i)\}_{i=1}^n$ of Ω as a *centroidal Voronoi tessellation* (CVT) if and only if the points $\{\mathbf{x}_i\}_{i=1}^n$ which serve as the generators of the associated Voronoi regions $\{V_i\}_{i=1}^n$ are also the centroids of those regions, i.e., if and only if we have that $\mathbf{x}_i = \mathbf{x}_i^*$ for $i = 1, \ldots, n$. The corresponding Delaunay triangulation is then called a *centroidal Voronoi Delaunay triangulation* (CVDT). CVTs are very useful in many applications, see [8] for details.

CVT and its duality CVDT based methods have attracted a lot of attention in the area of high-quality mesh generation and optimization, see [9, 10, 11]. When CVT/CVDT is applied to numerical solution of PDEs, e.g., in a finite element method or finite volume method, some modifications are needed to handle geometric constraints. An obvious one is that the CVT/CVDT mesh must conform with the boundary of the target domain Ω. Recently, a clear characterization of the influence of geometric constraints on the CVT-based meshing was proposed in [13]. Let us assume that the domain Ω is compact and $\partial\Omega$ is piecewise smooth with singular points $P_S = \{\mathbf{z}_i\}_{i=1}^k$. Denote by $\mathbf{proj}(\mathbf{x})$ the process that projects $\mathbf{x} \in \Omega$ to the point on the boundary closest to $\mathbf{x}$. Denote by P_I the set of generators whose voronoi regions are interior and by P_B the set of generators whose voronoi regions extend to the boundary, i.e., $P_I = \{\mathbf{x}_i \mid \overline{V_i} \cap \partial\Omega = \emptyset\}$ and $P_B = \{\mathbf{x}_i \mid V_i \cap \partial\Omega \neq \emptyset\}$. Then a Voronoi Tessellation $\{(\mathbf{x}_i, V_i)\}_{i=1}^n$ of Ω is called a *conforming centroidal Voronoi tessellation* (CfCVT) if and only if the following properties are satisfied:

- $P_S \subset \{\mathbf{x}_i\}_{i=1}^n$;
- $\mathbf{x}_i = \mathbf{x}_i^*$ if $\mathbf{x}_i \in P_I$;
- $\mathbf{x}_i = \mathbf{proj}(\mathbf{x}_i^*)$ if $\mathbf{x}_i \in P_B - P_S$.

The corresponding triangulation is called a *conforming centroidal Voronoi Delaunay triangulation*. Some efficient techniques for the construction of CfCVDTs in the two-dimensional space were proposed and implemented there using the so-called *constrained Delaunay triangulation* (CDT) process and a modified Lloyd type algorithm, see [8, 9, 10, 13] for details. Many sample CfCVDT meshes are also given in [13]. The three-dimensional implementation is still under development. Some other techniques for contructing CVT-based triangulations can be found in [10, 11]. An important and very useful relation pocessed by CVT/CVDT-based (or CfCVDT) meshes is that

$$\frac{h_i}{h_j} \approx \left(\frac{\rho(\mathbf{x}_j)}{\rho(\mathbf{x}_i)}\right)^{1/(d+2)}. \tag{3.2}$$

where h_i denotes the diameter of the Voronoi cell V_i, see [8, 11].

The CfCVDT meshes have been successfully used in [14] for adaptive computations of numerical solution of model second order elliptic PDEs. The main idea of our adaptive meshing algorithm for the solution of the steady incompressible Navier-Stokes equation (1.1) is similar to the one taken in

[14], i.e., to refine the old mesh and then optimize (or say re-mesh) it based on CfVDT algorithms according to some density function. A major advantage of this approach is that we may determine a density function ρ based on some posteriori error estimator and to generate the new mesh so that the errors of the new approximate solution will be equally distributed over the elements in an optimal way (i.e., with respect to the number of mesh nodes). Another advantage of this approach is that the resulted mesh always has good quality due to CVT's properties described above while most adaptive method often degenerates the mesh quality along the refinements.

3.2 Determination of the density function

Assume that we use the a posteriori error estimator η_T defined in (2.7) for the adaptive meshing. An important question then is how to determine a proper density function for the new CfVDT mesh $\mathcal{T}^{(\ell+1)}$ at the refinement level $(\ell+1)$ based on the local error estimator $\eta_T^{(\ell)}$ of the approximate solution at the previous mesh $\mathcal{T}^{(\ell)}$. A similar technique suggested in [14] can be derived. The basic idea is to construct a density function $\rho^{(\ell+1)}$ to adjust the local mesh size so that $\eta_T^{(\ell+1)}$ will be equally distributed as much as possible on each triangle $T \in \mathcal{T}^{(\ell+1)}$.

Let us define on each triangle $T \in \mathcal{T}^{(\ell)}$

$$\tilde{\rho}_T = \frac{\left(\eta_T^{(\ell)}\right)^{\frac{d+2}{k+2}}}{h_T^{d+2}}.$$

We then uniquely determine a piecewise linear function $\rho^{(\ell+1)}$ (with respect to $\mathcal{T}^{(\ell)}$) such that for any vertex $\mathbf{x}_i$ of $\mathcal{T}^{(\ell)}$,

$$\rho^{(\ell+1)}(\mathbf{x}_i) = \frac{\sum_{T\in S_i} \tilde{\rho}_T}{\mathrm{card}(S_i)} \tag{3.3}$$

where $S_i = \{T \in \mathcal{T}^{(\ell)} \mid \mathbf{x}_i \in \overline{T}\}$. Note that, if the local error estimator η_T and the prior estimate (2.4) are really good approximations to the true error locally, then we may assume that, there exists a contant c_T, depending on the position of T in the domain Ω, but independent of the size of T, such that

$$\eta_T^2 \approx c_T h_T^{2(k+1)+d} \tag{3.4}$$

The relation (3.4) is obtained by comparing the prior error estimate (2.4) with (2.8). Combining (3.4) with the CVT/CVDT property (3.2), it is then not difficult to verify that the CfCVDT mesh $\mathcal{T}^{(\ell+1)}$ generated by the density function $\rho^{(\ell+1)}$ will approximately have the property that

$$\eta_{T_i}^{(\ell+1)} \approx \eta_{T_j}^{(\ell+1)}$$

for any elements $T_i, T_j \in \mathcal{T}^{(\ell+1)}$.

The most time consuming step in the calculations of $\rho^{(\ell+1)}$ is the nearest neighbor search operation since they are defined by interpolation with respect to an unstructured mesh. However, this task can be efficiently solved using the software package "ANN" [1] as suggested in [14].

Remark 1 *For the INSE in two dimensional domains ($d = 2$), if the Hood-Taylor discretization is used, then we especially have*

$$\tilde{\rho}_T = \frac{\left(\eta_T^{(\ell)}\right)^{\frac{4}{3}}}{h_T^4}. \tag{3.5}$$

Remark 2 *The discussion above may not be applied to the cases in which the solution has strong anisotropy. See the discussion given in [14].*

3.3 Adaptive algorithm

Let $\mathcal{E}^{(\ell)} = \{E_i\}_{i=1}^{k^{(\ell)}}$ denote the set of edges of the ℓ-th level triangulation $\mathcal{T}^{(\ell)}$ and $k^{(\ell)}$ be the number of elements of $\mathcal{E}^{(\ell)}$. Set $\rho_{E_i} = \rho(\mathbf{z}_i)$ for any density function ρ, where $\mathbf{z}_i$ denotes the midpoint of the edge E_i. Let $CfCVDT(\mathcal{T}, \Omega, \rho)$ denote the construction algorithm for CfCVDT meshes taking $\mathcal{T}$ as the initial configuration for Ω and ρ as the density function. We can now define our adaptive meshing algorithm similar to the one used in [14] but with slight difference as follows.

Algorithm 1 *Given a domain Ω, an integer $N_{max} > 0$, an integer L_{max}, and a parameter $0 < \theta \leq 1$.*

0. *Generate an initial coarse triangulation $\mathcal{T}^{(0)}$ of Ω. Let $n^{(0)}$ denote the number of vertices of $\mathcal{T}^{(0)}$ and set $\ell = 0$.*

1. *Solve the INSE using the finite element method on $\mathcal{T}^{(\ell)}$. If $\ell > L_{max}$ or $n^{(\ell)} > N_{max}$, terminate; otherwise, go to step 2.*

2. *Determine the local error estimator $\eta_T^{(\ell)}$ for all $T \in \mathcal{T}^{(\ell)}$.*

3. *Construct $\rho^{(\ell+1)}$ using (3.3) and set the density function $\rho = \rho^{(\ell+1)}$. Determine $\{\rho_{E_i}\}_{i=1}^{k^{(\ell)}}$ and sort them in decreasing order.*

4. *Add $\{\mathbf{z}_i\}_{i=1}^{k_\theta}$ into the triangulation $\mathcal{T}^{(\ell)}$, where*

$$k_\theta = \max\Big\{k^* \;\Big|\; \sum_{i=1}^{k^*} \rho_{E_i} < \theta \sum_{i=1}^{k^{(\ell)}} \rho_{E_i}\Big\},$$

   and then form, the new intermediate triangulation $\widetilde{\mathcal{T}}^{(\ell+1)}$ with $n^{(\ell+1)} = n^{(\ell)} + k_\theta$ vertices.

5. *Optimize $\widetilde{\mathcal{T}}^{(\ell+1)}$ to obtain $\mathcal{T}^{(\ell+1)} = CfCVDT(\widetilde{\mathcal{T}}^{(\ell+1)}, \Omega, \rho)$, set $\ell \leftarrow \ell + 1$, then go to step 1.*

The parameter θ in Algorithm 1 is used here to control the refinement process [15]. The sorting procedure in step 4 can be implemented efficiently using a quick sorting algorithm.

Remark 3 *This adptive meshing scheme for INSEs also can be adapted to other discretizations and local a posteriori error estimators with appropriate changes on density functions.*

4 Numerical Experiments

In our numerical simulations, we only consider the two dimensional space and the Hood-Taylor scheme is used for the discretization of the INSEs (1.1) and (1.2). The CfCVDT mesh generator in [13] is used, which is implemented based on the "TRIANGLE" package [18]. We set $\theta = 0.3$ for all test problems. For our adaptive methods, the convergence rate CR with respect to the norm $\|\cdot\|$ at the refinement level ℓ is roughly computed by

$$\mathrm{CR} = \frac{2\log(\|e_{h,\ell}\|/\|e_{h,\ell-1}\|)}{\log(n_{\ell-1}/n_\ell)}, \tag{4.1}$$

where n_ℓ denotes the number of nodes and $\|e_{h,\ell}\|$ denotes the error $\|(\mathbf{u} - \mathbf{u}^h, p - p^h)\|_V$ at the refinement level ℓ or the global error estimator $\eta^{(\ell)}$ if the exact solution $(\mathbf{u}, p)$ is unknown. In order to evaluate the distribution of the local error estimator η_T over all elements of $\mathcal{T}$, we define the normalized standard deviation STD_{η_T} by

$$STD_{\eta_T} = \frac{\sqrt{\sum_{T\in\mathcal{T}} (\eta_T - \mathbf{E}\eta)^2/\text{card}(\mathcal{T})}}{\mathbf{E}\eta} \tag{4.2}$$

where $\mathbf{E}\eta$ denotes the expectation of η_T, i.e., $\mathbf{E}\eta = \sum_{T\in\mathcal{T}} \eta_T/\text{card}(\mathcal{T})$.

We apply the commonly used q measure to evaluate the quality of triangular meshes, where, for any triangle T, q is defined to be twice the ratio of the radius R_T of the largest inscribed circle and the radius r_T of the smallest circumscribed circle, i.e.,

$$q(T) = 2\frac{R_T}{r_T} = \frac{(b+c-a)(c+a-b)(a+b-c)}{abc},$$

where a, b, and c are side lengths of T. For a given triangulation $\mathcal{T}$, we define

$$q_{min} = \min_{T\in\mathcal{T}} q(T) \qquad \text{and} \qquad q_{avg} = \frac{1}{\text{card}(\mathcal{T})}\sum_{T\in\mathcal{T}} q(T) \tag{4.3}$$

where q_{min} will be used to measure the quality of the worst triangle and q_{avg} the average quality of the mesh $\mathcal{T}$.

4.1 Back-step problem

The first problem we tested is the so-called back-step problem where the domain was chosen to be $\Omega = ([-0.5, 9.5] \times [0, 0.5]) \cup ([0, 9.5] \times [-0.5, 0])$. The boundary conditions were set to be

$$\begin{aligned} &\mathbf{u}(x,y) = \begin{cases} (16y(0.5-y), 0), & \text{on the inflow boundary } \Gamma_i = \{-0.5\} \times [0, 0.5], \\ (0,0), & y = -0.5 \ \text{ or } \ y = 0.5 \ \text{ or } \ y = 0 \ \& \ -0.5 \le x \le 0, \end{cases} \\ &(\mathbf{u}\cdot\nabla)\mathbf{n} = 0, \qquad\qquad\qquad \text{on the inflow boundary } \Gamma_o = \{9.5\} \times [-0.5, 0.5]. \end{aligned} \tag{4.4}$$

We also chose the body force $\mathbf{f} = (0, 0)$ and the Reynold number $Re = \frac{1}{\nu} = 800$. It is known the exact solution $(\mathbf{u}, p)$ for this problem is smooth, i.e., $\mathbf{u} \in \mathbf{H}^3(\Omega)$ and $p \in H^3(\Omega)$ respectively. Since the exact solution is not obtainable, the convergence rate will be then computed based on the a posteriori error estimator η instead of the true error.

For this problem, we set $N_{max} = 10000$. The inital mesh and repeatedly refined CfCVDT meshes at some levels generated using Algorithm 1 for the back-step problem are shown in Figure 2. The distributions of nodes in the CfCVDT-based adaptive meshing process clearly show the accumulation of nodes in the vicinity of the origin and a strip close to the middle part of the domain from left to right. Table 1 reports information about mesh quality, error estimators and convergence rates at all refinement levels for this problem. The values of q_{min} and q_{avg} given in Table 1 demonstrate that the shape quality of the meshes resulting from the CfCVDT-based adaptive meshing strategy is always very good at all levels for the density functions ρ (3.3) defined based on the local a posteriori error estimator η_T, although the mesh sizes vary a lot over the Ω, e.g., h_{max}/h_{min} reaches 36.66 at the last level. It is also interested to observe h_{max}/h_{min} tends to monotonically increase for the adaptive methods. One also observes that our CfCVDT-based adaptive meshing method obtained very nice convergence rates along the refinements although they are not very stable at the beginning of refinements and also degerate a little at the last several levels. We believe it is partially due to the fact that ν is not small eonugh to obtain the perfect convergence rate 2.

An important optimal property of CfCVDT-based adaptive methods is the equi-distribution of the errors over all elements of the mesh. In order to verify this, we also pressent the values of STD_{η_T} defined in (4.2) at all refinement levels in Table 1. It is obvious that our adaptive meshing shceme does indeed distribute the errors more and more equally over all elements inflected by the decreasing of STD_{η_T} along the refinements. Finally, the approximate velocity and pressure fields $(\mathbf{u}^h, p^h)$ at the last refinement level are shown in Figure 3 for visualization purpose.

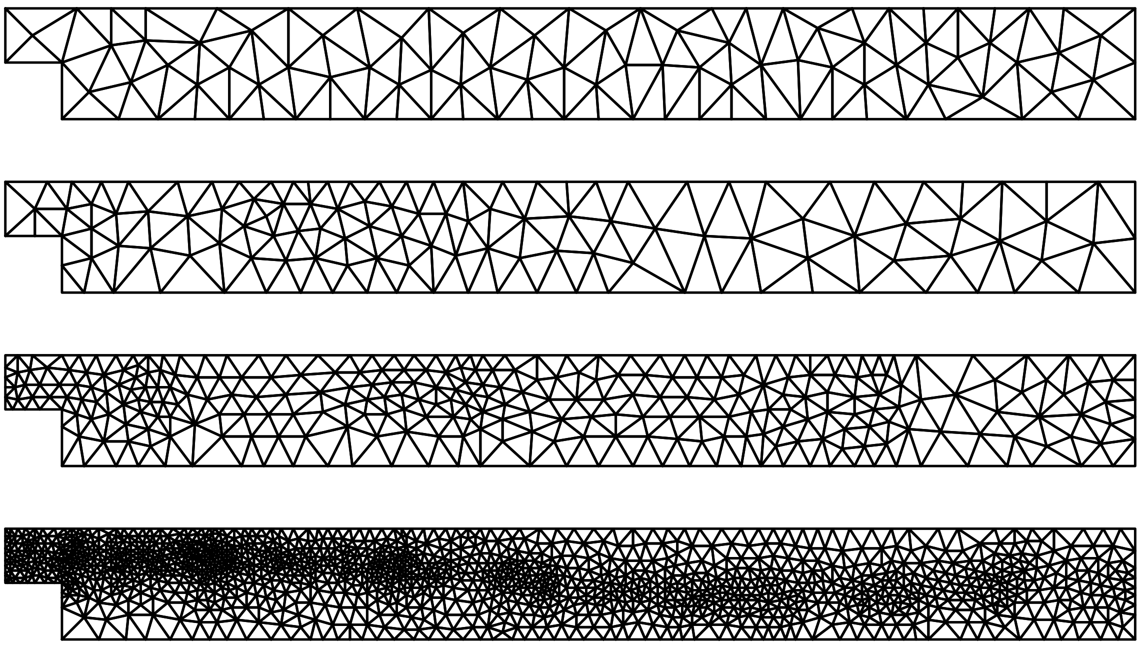

Figure 2: Adaptively refined meshes at some levels generated for the back-step problem. From top to bottom: initial mesh with 103 nodes and the CfCVDT meshes with 125, 301 and 1397 nodes, respectively.

4.2 Channel flow past a circular cylinder problem

The second problem we tested is the flow past a circular cylinder in a channel, abbreviated as the *cylinder* problem. Let a rectangle be given by $\Omega_1 = [-2, 20] \times [-2, 2.1]$ and a circle by $\Omega_2 = \{(x, y) \mid x^2 + y^2 < 0.5^2\}$, the target domain is then set to be $\Omega = \Omega_1 - \Omega_2$. We would like to remark that Ω is not symmetric with respect to the x-axis. The boundary condition is given by

$$
\begin{aligned}
&\mathbf{u}(x, y) = \begin{cases} \left(\frac{(2+y)(2.1-y)}{4.2}, 0\right), & \text{on the inflow boundary } \Gamma_i = \{-2.0\} \times [-2, 2.1], \\ (0, 0), & \text{on } \partial\Omega_2, \end{cases} \\
&(\mathbf{u} \cdot \nabla)\mathbf{n} = 0, \qquad \text{on the outflow boundary } \Gamma_o = \{20\} \times [-2, 2.1], \\
&v = 0 \quad \text{and} \quad \frac{\partial u}{\partial x} = 0, \qquad \text{on the top and bottom boundaries,}
\end{aligned}
\tag{4.5}
$$

where $\mathbf{u} = (u, v)$. We again let the body force $\mathbf{f} = (0, 0)$ and the Reynold number $Re = \frac{1}{\nu} = 200$ for this cylinder problem. It is well-known that the solutions $(\mathbf{u}, p)$ for this problem is not globally

ℓ	n_ℓ	q_{min}	q_{avg}	$\frac{h_{max}}{h_{min}}$	η	CR	STD_{η_T}
0	103	0.492	0.865	2.86	2.8732e-01	–	1.638
1	125	0.703	0.923	2.73	3.0376e-01	-0.575	1.763
2	149	0.624	0.918	4.66	1.7332e-01	6.390	1.630
3	183	0.666	0.932	4.04	9.9454e-02	5.405	1.260
4	234	0.664	0.930	3.71	7.1336e-02	2.703	1.498
5	301	0.655	0.931	4.67	4.8571e-02	3.053	1.224
6	396	0.660	0.932	5.43	4.4765e-02	0.595	1.324
7	522	0.709	0.936	7.53	3.6459e-02	1.486	1.285
8	697	0.508	0.934	5.96	2.1176e-02	3.759	0.987
9	971	0.618	0.939	6.61	1.6014e-02	1.686	0.912
10	1397	0.653	0.944	8.07	1.0422e-02	2.362	0.813
11	2048	0.555	0.939	8.87	7.3557e-03	1.822	0.747
12	3036	0.601	0.943	11.22	5.0480e-03	1.913	0.672
13	4609	0.550	0.942	16.22	3.4516e-03	1.821	0.600
14	7106	0.607	0.943	27.88	2.4270e-03	1.627	0.546
15	11076	0.567	0.944	36.66	1.7066e-03	1.687	0.485

Table 1: Mesh quality, error estimators, and convergence rates for the back-step problem.

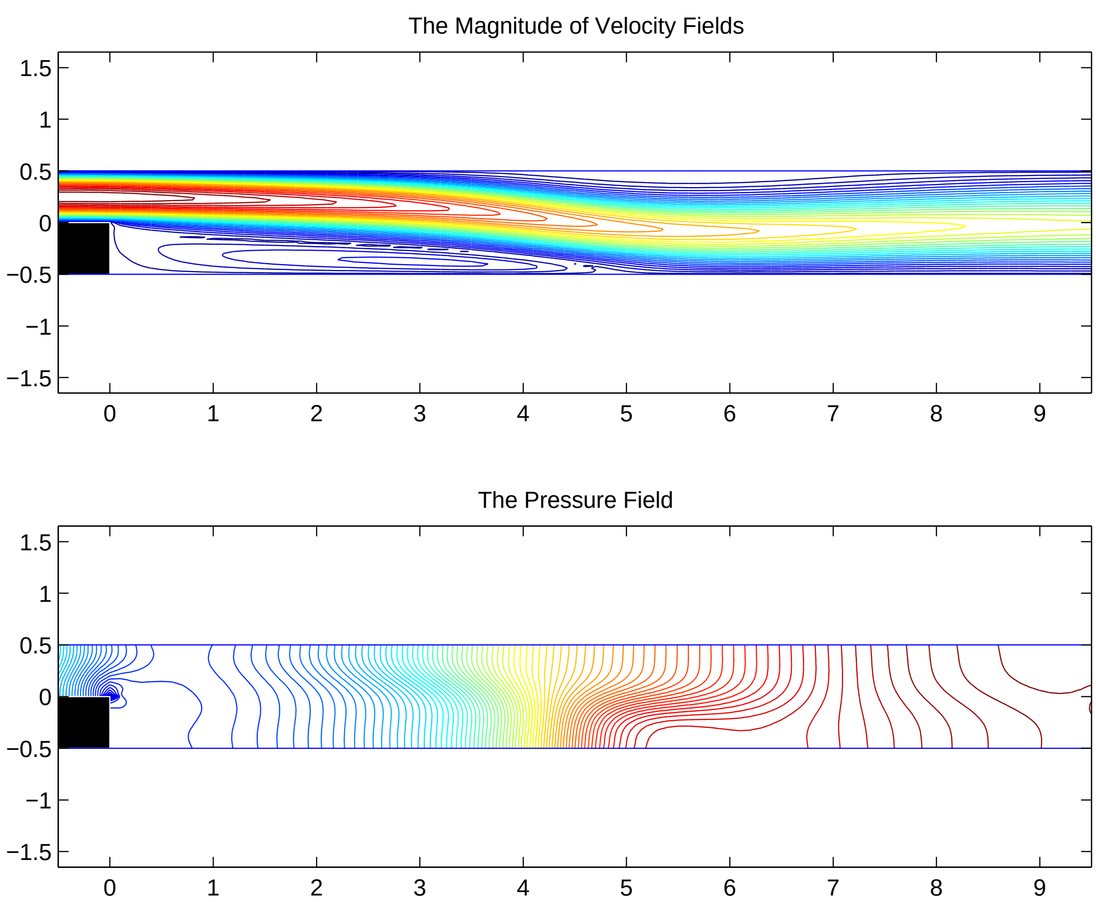

Figure 3: Plots of the approximate solution with 11076 nodes for the back-step problem. Top: the magnitude of velocity field $\mathbf{u}^h$; bottom: the pressure field p^h.

smooth, i.e., $\mathbf{u}$ and p only belong to $\mathbf{H}^1(\Omega)$ and $H^1(\Omega)$ respectively instead of $\mathbf{H}^2(\Omega)$ and $H^2(\Omega)$.

For this problem, we again set $N_{max} = 10000$. Due to the high sensitivity of the cylinder problem, we choose the intial mesh with more points concentrating around the cylinder to guarantee the convergence of the Newton's iteration. Figure 4 displays refined meshes at some levels generated by our CfCVDT-based adaptive meshing method. The distributions of nodes in the CfCVDT-adapted meshes clearly show the heavy accumulation of nodes near the region close to the left side of the cylinder and the sparsity near its right side. Table 2 reports information about mesh quality, error eatimators and convergence rates at all refinement levels for this cylinder problem. Again, all triangles are well shaped at all refinement levels, an observation that is supported by the values of q_{min} and q_{avg} listed in Table 2. At the same time, the values of h_{max}/h_{min} in Table 2 also shows the high variation of mesh sizes through the domain Ω, that reach the maximum 74.99 at the last level. Notice that this value 74.99 here is more than twice bigger than the one for the back-step problem due to the singularity of the exact solution. Although $\mathbf{u}$ and p are not smooth enough, the convergence rates obtained by our adaptive scheme are still as good as the ones for the back-step problem that has a smooth solution. From the values of STD_{η_T} list in Table 2, it is again obvious that our CfCVDT-based adaptive meshing method distributes the errors more and more equally over the triangles along the refinements. We finally display the representative approximate solution $(\mathbf{u}^h, p^h)$ at the last refinement level in Figure 5 for visulization.

ℓ	n_ℓ	q_{min}	q_{avg}	$\frac{h_{max}}{h_{min}}$	η	CR	STD_{η_T}
0	181	0.477	0.876	4.14	1.0590e+00	–	1.154
1	236	0.678	0.934	7.09	9.0408e-01	1.192	1.133
2	333	0.429	0.931	13.19	5.7878e-01	2.591	1.136
3	470	0.589	0.937	16.25	4.3911e-01	1.603	1.181
4	645	0.632	0.937	13.02	3.0286e-01	2.347	1.084
5	922	0.627	0.938	16.00	2.0164e-01	2.277	0.969
6	1339	0.651	0.941	23.44	1.2657e-01	2.496	0.935
7	1956	0.595	0.936	25.70	8.7698e-02	1.936	0.823
8	2924	0.593	0.941	26.74	5.8315e-02	2.029	0.705
9	4468	0.604	0.940	38.97	4.0594e-02	1.709	0.660
10	6848	0.576	0.941	53.84	2.8563e-02	1.646	0.588
11	10627	0.622	0.941	74.99	2.0117e-02	1.596	0.537

Table 2: Mesh quality, error estimators, and convergence rates for the cylinder problem.

4.3 Driven cavity problem

The third problem we tested is the so-called driven cavity problem. Let the domain be a square given by $\Omega = [-1, 1] \times [-1, 1]$ and set the pure Dirichlet boundary condition to be

$$\mathbf{u}(x, y) = \begin{cases} (1, 0), & [-1, 1] \times \{1\}, \\ (0, 0), & \text{otherwise}. \end{cases} \tag{4.6}$$

We also set the body force $\mathbf{f} = (0, 0)$ and the Reynold number $Re = \frac{1}{\nu} = 500$ for this problem. It is well-known that the solution $(\mathbf{u}, p)$ for this driven cavity problem satisfies $\mathbf{u} \notin \mathbf{H}^1(\Omega)$ and $p \notin H^1(\Omega)$. Especially, $\mathbf{u}$ and p have very strong singularity at the two top corners $(-1, 1)$ and $(1, 1)$ (It is easy to see that the velocity field $\mathbf{u}$ jumps there) but are smooth elsewhere. It is worth to point out that the discrete solution $(\mathbf{u}^h, p^h)$ will converge to the exact solution $(\mathbf{u}, p)$ only under the $\mathbf{L}^2 \times L^2$ norm, but not under the $\|\cdot\|_V$ norm. Consequently, the global error estimator η will

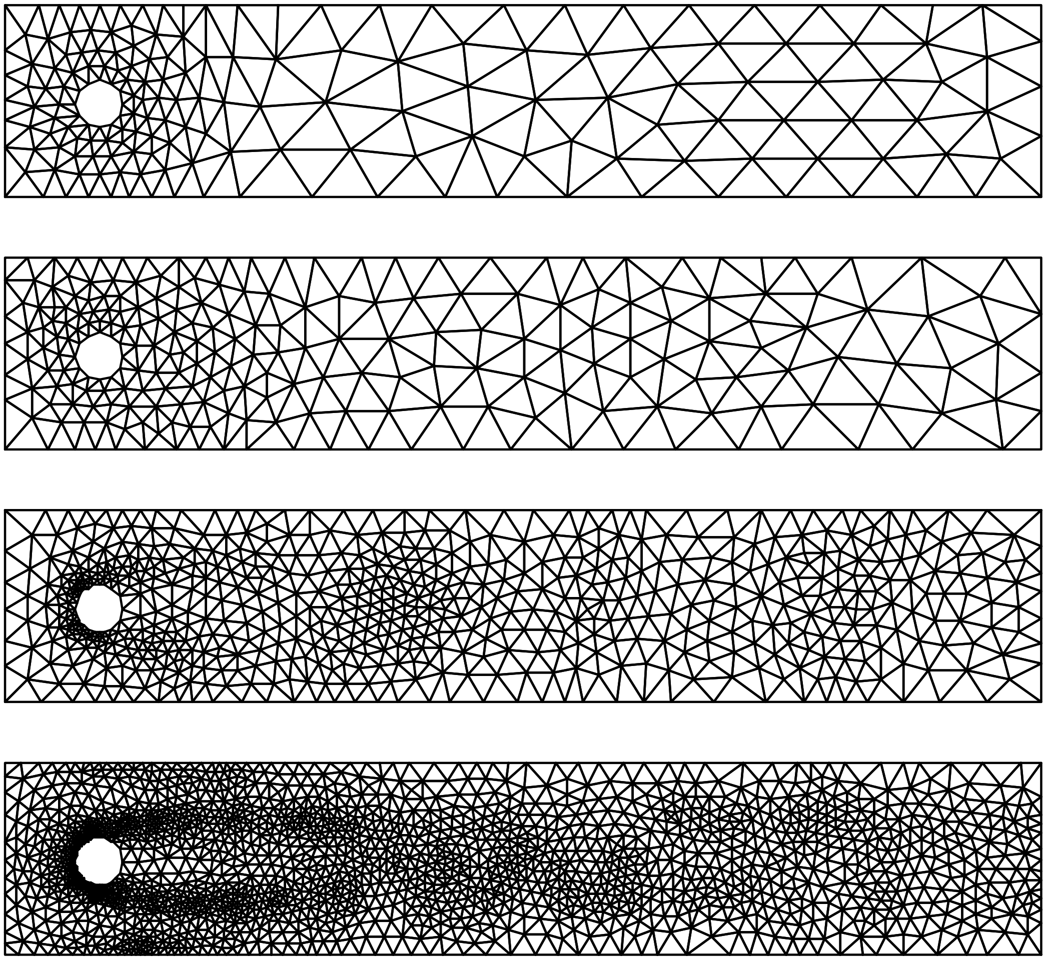

Figure 4: Adaptively refined meshes at some levels generated for cylinder problem. From top to bottom: initial mesh with 181 nodes and the CfCVDT meshes with 236, 645 and 1956 nodes, respectively.

not go to zero along the refinements. So we made the following changes to the local a posteriori error estimator η_T defined in (2.7):

$$\tilde{\eta}_T^2 = \eta_T^2 |T| \tag{4.7}$$

and $\tilde{\eta} = (\sum_{T\in\mathcal{T}} \tilde{\eta}_T^2)^{1/2}$. The above modification basically means that $\tilde{\eta}_T$ will be used to estimate the error $\|\mathbf{u} - \mathbf{u}^h\|_{0,\Omega} + \nu^{-2}\|p - p^h\|_{-1,\Omega}$ since the exact solution has less regularity. So it is more reasonable to use the $\tilde{\eta}_T$ in (3.5) for the determination of the density function ρ instead of η_T.

For this problem, we set $N_{max} = 5000$ since the domain is much smaller compared with former problems. The inital mesh and repeatedly refined CfCVDT meshes at some levels generated for the driven cavity problem are shown in Figure 6. The distributions of nodes in the CfCVDT-based adaptive meshes clearly show the accumulation of nodes near the points $(1, 1)$ and $(-1, 1)$ where the singularities in the solution occur, especially the latter one. Table 3 contains information about mesh quality, solution errors, and convergence rates at all refinement levels for the driven cavity problem. One sees that the CfCVDT-based adaptive methods still achieve excellent convergence rates with respect to $\tilde{\eta}$ although some instabilities show up at levels 12 and 14. Also, once again, all triangles remain well-shaped at all refinement levels, an observation that is supported by the values

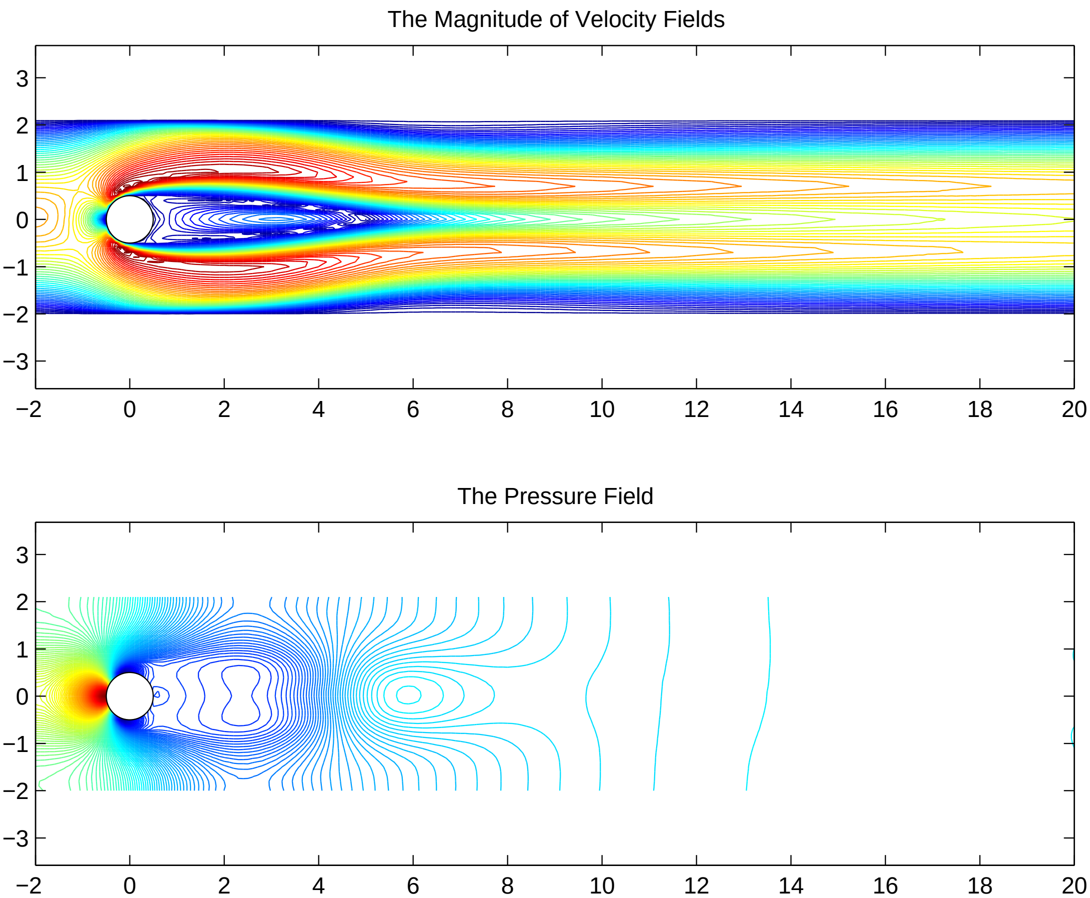

Figure 5: Plots of the approximate solution with 10596 nodes for the cylinder problem. Top: the magnitude of velocity field $\mathbf{u}^h$; bottom: the pressure field p^h.

of q_{min} and q_{avg} listed in Table 3 even though the mesh sizes vary greatly over the Ω, e.g., h_{max}/h_{min} reaches 160.31 at the last level. Notice that the value 160.31 here is much bigger than that for the back-step problem and the cylinder problem due to the much stronger singularity. The decreasing of $STD_{\tilde{\eta}_T}$ in 3 along the refinements again desmonstrates the effectiveness of our adaptive meshing scheme in distributing the errors more and more equally over all elements. We also display the approximate solution $(\mathbf{u}^h, p^h)$ at the last refinement level in Figure 7 for visualization purpose.

5 Conclusions

In this paper, we presented an efficient and robust adaptive mesh refining algorithm for solution of the steady incompressive Navier-Stokes equations using finite element approximations. Our meshing scheme combines a posteriori error estimation with the so-called conforming centroidal Voronoi Delaunay triangulation. The two ingredients are well connected together by the fact that the density function required by the second one is defined and computed from the first one. Various numerical experiments in two dimensions were carried out and showed that our meshing techniques worked very robust and obtained convergence rates (evaluated by the global a posteriori error estimate) close to the optimal one for the Hood-Taylor elements. This mesh adaptation strategy also can be easily generalized and applied to higher-order finite element approximations.

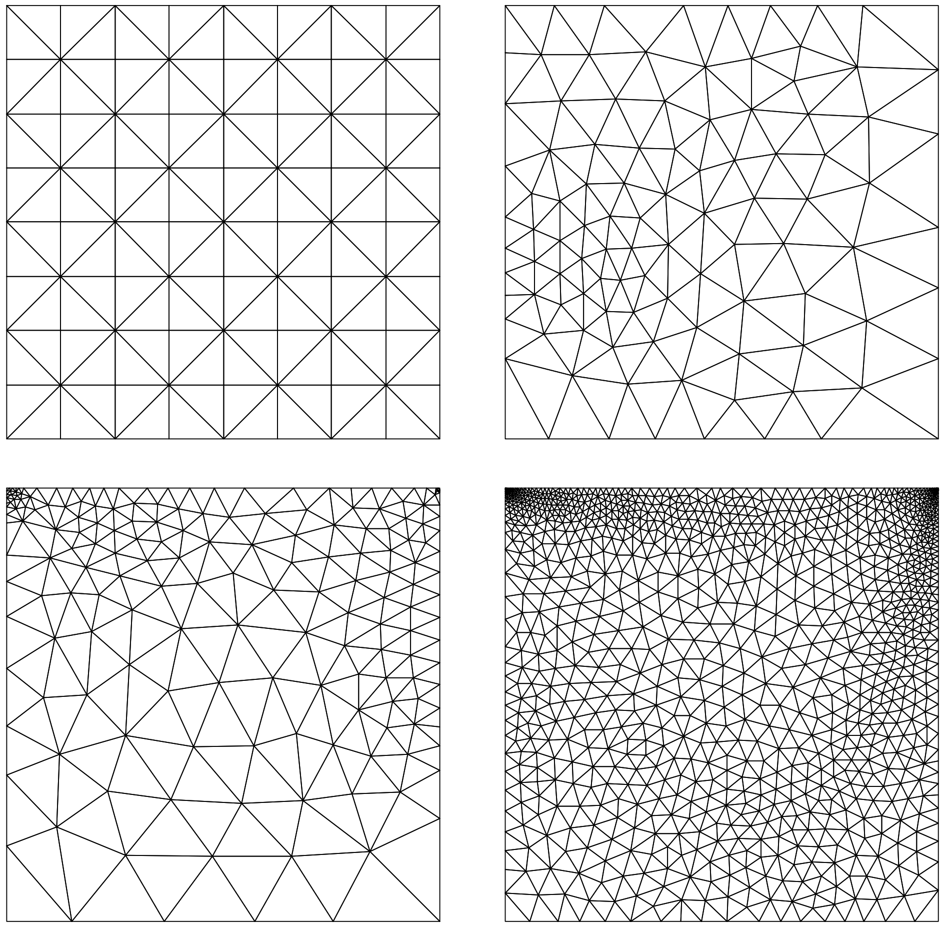

Figure 6: Adaptively refined meshes at some levels generated for the driven cavity problem. Top to bottom and left to right: initial mesh with 81 nodes and the CfCVDT meshes with 103, 193 and 1175 nodes, respectively.

References

[1] S. Arya and D. Mount, Approximate nearest neighbor searching, *Proceedings of 4th Ann. ACM-SIAM Symposium on Discrete Algorithms (SODA'93)* 1993, pp. 271-280.

[2] D. Arnica and C. Padra, A posteriori error estimators for the steady incompressible Navier-Stokes equations, *Numer. Meth. PDEs* **13**, 1998, pp. 561 - 574.

[3] M. Ainsworth and J. Oden, *A Posteriori Error Estimation in Finite Element Analysis*, Wiley, 2002.

[4] I. Babuska and A.D. Miller, A feedback finite element method with a posteriori error estimation Part I, *Comput. Meth. Appl. Mech. Engrg* **61**, 1987, pp. 1-40.

[5] I. Babuska and W.C. Rheinboldt, Error estimates for adaptive finite element computations, *SIAM J. Numer. Anal.* **15**, 1978, pp. 736–754.

[6] Babuska and W.C. Rheinboldt, A posteriori error analysis of finite element solutions for one dimensional problems, *SIAM J. Numer. Anal.* **18**, 1981, pp. 565-589.

ℓ	n_ℓ	q_{min}	q_{avg}	$\frac{h_{max}}{h_{min}}$	$\tilde{\eta}$	CR	$STD_{\tilde{\eta}_T}$
0	81	0.828	0.828	1.00	4.8359e+00	–	1.409
1	103	0.709	0.931	3.93	1.0031e-01	32.258	1.486
2	125	0.491	0.911	4.82	1.2828e-02	21.247	2.398
3	137	0.536	0.911	16.25	8.5610e-03	8.823	1.807
4	155	0.558	0.909	28.93	5.3056e-03	7.751	1.278
5	193	0.350	0.904	57.45	3.3694e-03	4.141	0.980
6	249	0.274	0.901	48.29	2.0454e-03	3.918	0.806
7	343	0.400	0.924	42.23	1.1905e-03	3.379	0.594
8	505	0.586	0.936	48.39	7.4202e-04	2.444	0.633
9	767	0.513	0.933	62.43	4.4451e-04	2.452	0.620
10	1175	0.421	0.938	61.29	2.8471e-04	2.088	0.677
11	1835	0.638	0.938	88.11	1.6954e-04	2.326	0.612
12	2868	0.621	0.942	76.24	1.3168e-04	1.132	1.072
13	4539	0.652	0.943	145.50	6.7523e-05	2.910	0.708
14	5708	0.661	0.943	160.31	5.9412e-05	1.117	0.664

Table 3: Mesh quality, error estimators, and convergence rates for the driven cavity problem.

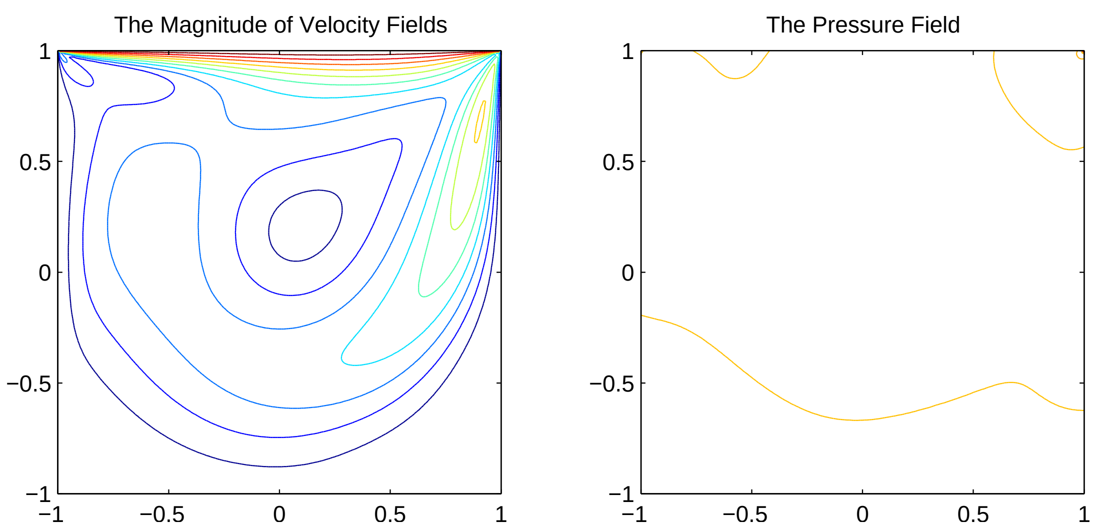

Figure 7: Plots of the approximate solution with 5708 nodes for the driven cavity problem. Top: the magnitude of velocity field $\mathbf{u}^h$; bottom: the pressure field p^h.

[7] W. Dörfler, A convergent adaptive algorithm for Poisson's equation. *SIAM J Numer. Anal.* **33**, 1996, pp. 1106-1124.

[8] Q. Du, V. Faber, and M. Gunzburger, Centroidal Voronoi tessellations: Applications and algorithms, *SIAM Review* **41**, 1999, pp. 637-676.

[9] Q. Du and M. Gunzburger, Grid generation and optimization based on centroidal Voronoi tessellations, *Applied Math. Comptut.* **133**, 2002, pp. 591-607.

[10] Q. Du and D. Wang, Tetrahedral mesh generation and optimization based on centroidal Voronoi tessellations, *Int. J. Numer. Methods Engrg.* **56**, 2003, pp. 1355-1373.

[11] Q. Du and D. Wang, On the optimal centroidal Voronoi tessellations and the Gersho's conjecture in the Three Dimensional Space, *Computer and Mathematics with Applications* **49**, 2005, pp. 1355-1373.

[12] V. Girault and P.A. Raviart, *Finite Element Methods for Navier-Stokes Equations*, Springer, Berlin, 1986.

[13] L. Ju, Conforming centroidal Voronoi Delaunay triangulation for quality mesh generation, *Inter. J. Numer. Anal. Model.*, to appear.

[14] L. Ju, M. Gunzburger, and W.-Z. Zhao, Adaptive finite element methods for elliptic PDEs based on conforming centroidal Voronoi Delaunay triangulations, *SIAM J. Sci. Comput.* **28**, 2006, pp. 2023-2053.

[15] P. Morin, R.H. Nochetto, and K.G. Siebert, Data oscillation and convergence of adaptive FEM, *SIAM J. Numer. Anal.* **38**, 2000, pp. 466-488.

[16] P. Morin, R.H. Nochetto, and K.G. Siebert, Local problems on stars: A posteriori error estimators, convergence, and performance, *Math. Comp.* **72**, 2003, pp. 1067-1097.

[17] J.T. Oden, W. Wu, and M. Ainsworth, An a posteriori error estimate for finite element approximations of the Navier-Stokes equations, *Comput. Meths. Appl. Mech. Engrg.* **111**, 1994, pp. 185-202.

[18] J. Shewchuk, Triangle: Engineering a 2D quality mesh generator and Delaunay triangulator, *Lecture Notes in Comput. Sci.* **1148**, Springer, New York, 1996, pp. 203-222.

[19] R. Temam, *Navier-Stokes Equations*, North-Holland, Amsterdam, 1984.

[20] R. Verfurth, A posteriori error estimates for non-linear problems: Finite element discretizations of elliptic equations, *Math. Comp.* **62**, 1994, pp. 445-475.